JOURNAL OF MECHANICS OF CONTINUA AND MATHEMATICAL SCIENCES
www.journalimcms.org

ISSN (Online) : 2454 -7190 Vol.-21, No.-06, June (2026) pp 96-113 ISSN (Print) 0973-8975

VIBRATIONS OF RIGIDLY FIXED NONLOCAL THERMOELASTIC CYLINDRICAL STRUCTURE WITH DOUBLE POROSITY

Savita Katoch[1], Dinesh Kumar Sharma[2], Vikas Sharma[3] Nivedita Sharma[4]

[1,2] Department of Mathematics, Maharaja Agrasen University, Baddi, Solan, Himachal Pradesh – 174103, India.

[3]School of Engineering and Technology, Mathematics Department, CGC University, Mohali, Punjab - 140307 India.

[4]Department of Mathematics, Faculty of Science, Dayalbagh Educational Institute (DEI), Deemed to be University, Agra, 282005, India.

Emails: katochsavita5@gmail.coms, dksharma200513@gmail.com, vikusharma168@gmail.com, nivi2j@gmail.com

Corresponding Author: **Dinesh Kumar Sharma**

https://doi.org/10.26782/jmcms.2026.06.00005

(Received: March 23, 2026; Revised: June 03, 2026; Accepted: June 14, 2026)

Abstract

Objective: *The investigation of a nonlocal elastic hollow cylinder with double porosity has been presented for rigidly fixed boundary conditions in the context of generalized thermoelasticity. Governing equations are transformed into ordinary differential equations through harmonics variation technique.*

Methods: *The system of equations is solved with the help of the matrix elimination approach, which yields a characteristic equation of eighth degree. The unknown field functions for dilatation, porosity, temperature, and displacement have been shown analytically. Analytical results are verified through numerical simulations by Computer based MATLAB software by using Iteration numerical technique. Generated data through simulations corresponds to the roots of the equation, termed the mode number.*

Results: *The generated data is of the form complex numbers, which reveals that the real part is known as the natural frequency, and the imaginary part represents the damping factor. The computer analysed and generated data has been presented graphically for frequency shift, thermoelastic damping, and field functions such as displacement, porosity, and temperature. The generated data has also been shown in tables for natural frequencies.*

Conclusions: *The findings of the study have potential relevance in smart materials, nanotechnology, biomedical implants, energy storage systems, and aerospace components*.

Keywords: Porosity, Thermoelasticity, Free vibrations, Natural frequency, Frequency shift, Rigidly fixed boundaries.

I. Introduction

Elasticity with porous structures and thermal effects is an essential constitutive relation for the materials, which enables them to deform under the action of external forces and entirely recover their original configuration upon unloading. Achenbach [I] presented elastic wave propagation theory, covering three-dimensional elastodynamics, wave phenomena, and mathematical methods. Ciarletta and Sumbatyan [II] studied inclined plane wave reflection analysis from free surfaces in elastic solids with voids. Cowin and Nunziato [III] examined linear elasticity theory for materials with voids and capturing deformations. Dhaliwal and Singh [IV] had given a detailed look into lots of problems of elasticity and thermoelasticity in the context of continuum mechanics. Eringen [V] discussed the principles of nonlocal thermodynamical problems by incorporating significant surface physics effects. Extensive research work with the analysis of elastic waves at the boundaries in classical elastic media, with foundational contributions, was examined by Ewing et al. [VI]. Gupta et al. [VII] discussed the two-dimensional thermo-mechanical response of micropolar double-porous nonlocal thermoelastic materials using the Moore-Gibson-Thompson (MGT) heat conduction equation. Iesan and Quintanilla [VIII] developed thermoelastic theory for double-porous solids in the framework of the Cowin-Nunziato model. Iesan [IX] developed a linear theory of thermoelastic materials with voids, establishing uniqueness, reciprocal, variational theorems, acceleration waves, and equilibrium problems. Ismail et al. [X] discussed two-dimensional nonlocal thermoelastic analysis of double-porosity semiconductors under photo-thermal excitation and revealed the effects of dual porosity. Kansal [XI] investigated anisotropic thermoelastic media with double porosity and micro-temperatures for various parameters. Lord and Shulman (LS) [XII] formulated a generalized dynamical thermoelasticity theory by incorporating heat flow acceleration time, ensuring hyperbolic coupled equations, and eliminating the infinite velocity of propagation paradox. Parra et al. [XIII] studied acoustic wave propagation in gas-saturated double-porosity meta-materials, highlighting exotic effective fluid properties. Pathania et al. [XIV] analyzed plane waves in a rotating thermoelastic double-porous medium, revealing five coupled modes with analytical amplitudes and numerical validation. Sharma et al. [XV] studied free vibrations of a nonlocal thermoelastic cylinder with voids to present a graphical representation for thermoelastic damping and frequency shift. Sharma et al. [XVI] examined the transient wave vibrations of a viscoelastic cylindrical structure with double porosity and presented field functions graphically. Sharma et al. [XVII] studied a functionally graded thermoelastic cylinder for free vibration analysis and presented the results for thermoelastic damping, frequency shift, and natural frequencies. Sharma et al. [XVIII] investigated the variable thermal conductivity effects in an axisymmetric

isotropic cylinder using the MGT thermoelastic model. Svanadze [XIX] discussed elastic wave behavior in porous solids and proved the uniqueness and existence of boundary value solutions. Yahya and Abd-Alla [XX] analyzed radial vibrations of a rotating elastic hollow cylinder, deriving frequency equations under different boundary conditions, and presented the eigenvalues and dispersion relations numerically. Yildirim and Esen [XXI] examined the thermo-mechanical response of high-porosity functionally graded nanoplates under extreme temperature and humidity with various field functions Zhong et al. [XXII] discussed viscoelastic polymer flooding in porous media using computational fluid dynamics for the oil recovery efficiency.

The present paper investigates the analysis of a nonlocal thermoelastic cylinder with double porosity, capturing microstructural interactions and heat conduction effects to present the vibrations in the context of rigidly fixed boundary conditions. The problem has been modeled with Lord and Shulman (LS) [XII] model of generalized thermoelasticity. Results highlight the critical role of porosity distribution and nonlocal parameters in controlling wave propagation stability and dynamic response. The generated data has been presented graphically for frequency shift and thermoelastic damping as a function of mode number. The generated data has also been shown in tables for natural frequencies. The study may find applications in smart materials, nanotechnology, biomedical implants, energy storage systems, and aerospace components.

II. Formulation of the Problem

The analysis of a homogenous isotropic nonlocal thermoelastic cylinder has been presented for rigidly fixed vibrations in the context of double porosity with a domain $a \le r \le \eta a$. The cylindrical coordinates (r, θ, z) have been shown for field function components as $\boldsymbol{u} = (u(r,t)\ ,\ 0\ ,\ 0)$, $\phi = \phi(r,t)$ and $\psi = \psi(r,t)$. Here the terms $\boldsymbol{u} = u(r,t)$, $\phi(r,t)$ and $\psi(r,t)$ are denoted as displacement vector, macro porosity, and micro porosity, respectively. The temperature component term has been denoted as $\theta(r,t)$. The macro-porosity parameter influences the global stiffness reduction and leads to a noticeable decrease in the eigenfrequencies. In contrast, the micro-porosity parameter affects the local inertia and microstructural interaction effects, resulting in comparatively subtler but mode-dependent variations in the vibrational response. The governing equations are presented in the absence of body forces and without heat sources (Eringen [V], Cowin and Nunziato [III], Iesan [IX], and Dhaliwal and Singh [IV]) are given as under:

$$\frac{\partial \sigma_{rr}}{\partial r} + \frac{1}{r}\left(\sigma_{rr} - \sigma_{\theta\theta}\right) = \rho(1 - \varepsilon^2 \nabla^2)\frac{\partial^2 u}{\partial t^2}\,, \tag{1}$$

$$\alpha \nabla^2 \phi + b_1 \nabla^2 \psi - be - \alpha_1 \left(1 + \phi_0 \frac{\partial}{\partial t}\right)\phi - \alpha_3 \psi + \beta_1 \theta = \chi_1 (1 - \varepsilon^2 \nabla^2)\frac{\partial^2 \phi}{\partial t^2}\,, \tag{2}$$

$$b_1 \nabla^2 \phi + \gamma \nabla^2 \psi - de - \alpha_3 \phi - \alpha_2 \left(1 + \psi_0 \frac{\partial}{\partial t}\right)\psi + \beta_2 \theta = \chi_2 (1 - \varepsilon^2 \nabla^2)\frac{\partial^2 \psi}{\partial t^2}\,, \tag{3}$$

$$K\nabla^2\theta-\rho c_e\left(\frac{\partial}{\partial t}+t_0\frac{\partial^2}{\partial t^2}\right)\theta=\left(\frac{\partial}{\partial t}+t_0\frac{\partial^2}{\partial t^2}\right)(\beta_1T_0\phi+\beta_2T_0\psi+\beta_eT_0e)=0\,, \tag{4}$$

$$(1-\varepsilon^2\nabla^2)\sigma_{ij}=\sigma_{ij}^L=2\mu e_{ij}+(\lambda e_{ij}+b\phi+d\psi)\delta_{ij}-\beta_e\theta\,, \tag{5}$$

$$e_{ij}=\frac{u_{i,j}+u_{j.i}}{2}\;;(i,j=r,\theta,z) \tag{6}$$

where $e_{ij}(i,j=r,\theta,z)$ are strain components, $\sigma_{ij}(i,j=r,\theta,z)$ are stresses, ρ is mass density, λ and μ are Lame's constants, ε is elastic nonlocal parameter, $\alpha,\gamma,\alpha_1,\alpha_2,\alpha_3,b,b_1,d$ are the constitutive voids coefficients, $e=e_{rr}+e_{\theta\theta}+e_{zz}$ is cubical dilatation, χ_1 and χ_2 are the coefficients of equilibrated inertia corresponding to voids of macro and micro porosity respectively, K is thermal conductivity, θ is temperature increment, c_e states for specific heat at constant strain, $\beta_e=(3\lambda+2\mu)\alpha_T$, α_T is linear thermal expansion, T_0 is reference temperature, β_e,β_1,β_2 are thermoelastic coupling coefficients respectively. Substituting components from equations (5) and (6) in equation (1), and on rearrangement of the equation, provides us

$$\nabla^2e+b_{01}\nabla^2\phi+d_{01}\nabla^2\psi-\bar{\beta}_e\nabla^2\theta=(1-\varepsilon^2\nabla^2)\frac{\partial^2e}{\partial t^2} \tag{7}$$

where

$$b_{01}=\frac{b}{\lambda+2\mu},\;d_{01}=\frac{d}{\lambda+2\mu},\;\bar{\beta}_e=\frac{\beta_eT_0}{\lambda+2\mu}.$$

III. Solution of the Problem

We propose the following non-dimensional parameters to remove the complexity of the governing equations:

$$\begin{cases}(u',r',\varepsilon_0)=\dfrac{1}{a}(u,r,\varepsilon),(\tau,\tau_0,\phi_0',\psi_0')=\dfrac{c_1}{a}(t,t_0,\phi_0,\psi_0),c_1^2=\dfrac{\lambda+2\mu}{\rho}\\ c_2^2=\dfrac{\mu}{\rho},(\tau_{rr},\tau_{\theta\theta})=\dfrac{(\sigma_{rr},\sigma_{\theta\theta})}{\rho c_1^{\,2}}\,,\;\phi'=\dfrac{\chi_1\Omega^{*2}}{a^2}\phi,\psi'=\dfrac{\chi_2\Omega^{*2}}{a^2}\psi\,,\;\theta'=\dfrac{\theta}{T_0}\end{cases} \tag{8}$$

Here $\Omega^*=\dfrac{\omega^*a}{c_1}$ is the characteristic frequency of the medium, $\omega^*=\dfrac{c_e(\lambda+2\mu)}{K}$ is the angular frequency, c_1 , c_2 and are the longitudinal and shear wave speeds. Plugging the parameters from equation (8) into equations (2) to (5) and (7), we have

$$\nabla^2e-(1-\varepsilon_0^2\nabla^2)\frac{\partial^2e}{\partial^2\tau}+b_{01}^*\nabla^2\phi+d_{01}^*\nabla^2\psi-\bar{\beta}_e\nabla^2\theta=0 \tag{9}$$

$$-a_2^*e+\left(\nabla^2-a^*\left(1+\phi_0\frac{\partial}{\partial\tau}\right)\right)\phi-\left(1-\varepsilon_0^2\nabla^2\right)\frac{1}{\delta_1^2}\frac{\partial^2\phi}{\partial\tau^2}+(a_1^*\nabla^2-a_3^*)\psi+\beta_1^*\theta=0 \tag{10}$$

$$-a_7^*e+\left(a_4^*\nabla^2-a_5^*\right)\phi+\left(\nabla^2-a_6^*\left(1+\psi_0\frac{\partial}{\partial\tau}\right)\right)\psi-\left(1-\varepsilon_0^{\,2}\nabla^2\right)\frac{1}{\delta_2^{\,2}}\frac{\partial^2\psi}{\partial\tau^2}+\beta_2^*\theta=0 \tag{11}$$

$$\left[\theta^*e+\chi_1^*\phi+\chi_2^*\psi\right]\left(\frac{\partial}{\partial\tau}+\tau_0\frac{\partial^2}{\partial\tau^2}\right)-\left(\nabla^2-\Omega^*\left(\frac{\partial}{\partial\tau}+\tau_0\frac{\partial^2}{\partial\tau^2}\right)\right)\theta=0 \tag{12}$$

where

$$e=\frac{\partial u}{\partial r}+\frac{u}{r},\ b_{01}^*=\frac{b_{01}a^2}{\chi_1\Omega^{*^2}},\ d_{01}^*=\frac{d_{01}a^2}{\chi_2\Omega^{*^2}},\beta_1^*=\frac{\beta_1\chi_1\Omega^{*^2}}{a^2\alpha},\ \beta_2^*=\frac{\beta_2\chi_2\Omega^{*^2}}{a^2\gamma},a^*=\frac{\alpha_1}{\alpha}$$

$$a_1^*=\frac{b_1\chi_1}{\alpha\chi_2},\ a_2^*=\frac{b\chi_1\Omega^{*^2}}{\alpha a^2},a_3^*=\frac{\alpha_3\chi_1}{\alpha\chi_2},\ a_4^*=\frac{b_1\chi_2}{\gamma\chi_1},a_5^*=\frac{\alpha_3\chi_2}{\gamma\chi_1},a_6^*=\frac{a_2}{\gamma},a_7^*=\frac{d\chi_2\Omega^{*^2}}{\gamma a^2}$$

$$\delta^2=\frac{\mu}{\lambda+2\mu},\delta_1^{\,2}=\frac{\alpha}{c_1^{\,2}\Omega^{*^2}},\ \delta_2^{\,2}=\frac{\gamma}{c_1^{\,2}\Omega^{*^2}},\ \chi_1^{\,*}=\frac{\beta_1c_1^2a^2}{K\chi_1\omega^*},\ \chi_2^{\,*}=\frac{\beta_2c_1^2a^2}{K\chi_2\omega^*},\ \theta^*=\frac{\varepsilon_T\Omega^*}{\bar{\beta}_e},\ \varepsilon_T=\frac{\beta_e^2T_0}{\rho c_e(\lambda+2\mu)}$$

Primes (‘) have been suppressed for convenience. For the simplicity of equations, we propose time harmonic vibrations as given below:

$$(e\quad\phi\quad\psi\quad\theta)=(\bar{e}\quad\bar{\phi}\quad\bar{\psi}\quad\bar{\theta})\exp\left(-i\Omega\tau\right). \tag{13}$$

Here $\Omega=\dfrac{\omega a}{c_1}$ is the non-dimensional circular frequency of the vibrations, ω is the circular frequency of the medium. Upon using time harmonics assumed from equation (13) in equations (5) and (9) to (12), we obtained

$$\begin{pmatrix}(\nabla^2+b_{11}) & b_{12}\nabla^2 & b_{13}\nabla^2 & b_{14}\nabla^2\\ -b_{21} & (\nabla^2+b_{22}) & (B^*\nabla^2-b_{23}) & b_{24}\\ -b_{31} & (B_1^{\,*}\nabla^2-b_{32}) & (\nabla^2+b_{33}) & b_{34}\\ b_{41} & b_{42} & b_{43} & (\nabla^2-b_{44})\end{pmatrix}\begin{pmatrix}\bar{e}\\ \bar{\phi}\\ \bar{\psi}\\ \bar{\theta}\end{pmatrix}=\begin{pmatrix}0\\0\\0\\0\end{pmatrix}, \tag{14}$$

$$\begin{cases}\tau_{rr}=e-2\delta^2\dfrac{u}{r}+b_{01}^*\phi+d_{01}^*\psi-\bar{\beta}_e\theta\\ \tau_{\theta\theta}=(1-2\delta^2)e+2\delta^2\dfrac{u}{r}+b_{01}^*\phi+d_{01}^*\psi-\bar{\beta}_e\theta\end{cases}, \tag{15}$$

where

$$b_{11}=\frac{\Omega^{^2}}{1-\Omega^2\varepsilon_0^2},b_{12}=\frac{b_{01}^*}{1-\Omega^2\varepsilon_0^2},b_{13}=\frac{d_{01}^*}{1-\Omega^2\varepsilon_0^2},b_{14}=\frac{\bar{\beta}_e}{1-\Omega^2\varepsilon_0^2},$$

$$b_{21}=\frac{a_2^*\delta_1^2}{\delta_1^2-\varepsilon_0^2\Omega^2},b_{22}=a^*i\Omega\phi_0^*-\frac{\Omega^2}{\delta_1^2},b_{23}=\frac{a_3^*\delta_1^2}{\delta_1^2-\varepsilon_0^2\Omega^2},b_{24}=\frac{\beta_1^{\,*}\delta_1^2}{\delta_1^2-\varepsilon_0^2\Omega^2},$$

$$b_{31}=\frac{a_7^*\delta_2^2}{\delta_2^2-\varepsilon_0^2\Omega^2},\ b_{32}=\frac{a_5^*\delta_2^2}{\delta_2^2-\varepsilon_0^2\Omega^2},\ b_{33}=a_6^*i\Omega\psi_0^*-\frac{\Omega^2}{\delta_2^2},\ b_{34}=\frac{\beta_2^*\delta_2^2}{\delta_2^2-\varepsilon_0^2\Omega^2},$$

$$b_{41}=\theta^{*}\Omega^{2}\tau_{0}^{*},\ b_{42}=\Omega^{2}\chi_{1}^{*}\tau_{0}^{*},\ b_{43}=\Omega^{2}\chi_{2}^{*}\tau_{0}^{*},\ b_{44}=-\Omega^{*}\Omega^{2}\tau_{0}^{*},\ B^{*}=\frac{a_{1}^{*}\delta_{1}^{2}}{\delta_{1}^{2}-\varepsilon_{0}^{2}\Omega^{2}},$$

$$B_{1}^{*}=\frac{a_{4}^{*}\delta_{2}^{2}}{\delta_{2}^{2}-\varepsilon_{0}^{2}\Omega^{2}},\ \phi_{0}^{*}=i\Omega^{-1}+\phi_{0},\ \psi_{0}^{*}=i\Omega^{-1}+\psi_{0},\ \tau_{0}^{*}=i\Omega^{-1}+\tau_{0}.$$

In order to evaluate the unknown parameters $\bar{e},\bar{\phi},\bar{\psi},\bar{\theta}$ by solving equation (14), we obtain a characteristic equation satisfying $\bar{e},\bar{\phi},\bar{\psi},\bar{\theta}$ as follows:

$$\left(\nabla^{8}+A\nabla^{6}+B\nabla^{4}+C\nabla^{2}+D\right)\left(\bar{e},\bar{\phi},\bar{\psi},\bar{\theta}\right)^{'}=0, \tag{16}$$

where $A=\frac{A_{1}}{(B^{*}B_{1}^{*}-1)},B=\frac{B_{1}}{(B^{*}B_{1}^{*}-1)},C=\frac{C_{1}}{(B^{*}B_{1}^{*}-1)},D=\frac{D_{1}}{(B^{*}B_{1}^{*}-1)}.$

Here, the parameters A_{1} , B_{1}, C_{1} , D_{1} are defined in Appendix (A1.1) to (A1.4). The equation (16) is bi-quadratic in ∇^{2} and may be factorized as

$$(\nabla^{2}+k_{1}^{2})(\nabla^{2}+k_{2}^{2})(\nabla^{2}+k_{3}^{2})(\nabla^{2}+k_{4}^{2})(\bar{e},\bar{\phi},\bar{\psi},\bar{\theta})^{'}=0 \tag{17}$$

Here k_{1}^{2} , k_{2}^{2} , k_{3}^{2} and k_{4}^{2} are the roots of the following characteristic equation:

$$k^{8}+Ak^{6}+Bk^{4}+Ck^{2}+D=0. \tag{18}$$

Equation (18) is bi-quadratic in k^{2} provides us eight roots for k , which have the property $k_{2}=-k_{1}$, $k_{4}=-k_{3}$, $k_{6}=-k_{5}$, $k_{8}=-k_{7}$, and satisfy the radiation condition, i.e. $\mathrm{Re}(k_{i})\geq 0;(i=1,\ 2,\ 3,\ 4)$. The eigenvalue problem governing free vibrations is explicitly dependent on the nonlocal parameter through the modified constitutive relations and governing equations. As a result, the stiffness characteristics of the system are effectively reduced with increasing nonlocal parameter, leading to a corresponding decrease in the eigenfrequencies. The analysis reveals that the eigenfrequencies exhibit a monotonic decreasing trend with increasing nonlocal parameter, which is consistent with the softening effect induced by nonlocal interactions. This behavior becomes more pronounced for higher modes, indicating greater sensitivity of higher-order eigen frequencies to nonlocal effects due to their increased spatial gradients. Therefore, the solutions of equation (16) are as follows:

$$\begin{pmatrix}\bar{e}\\ \bar{\phi}\\ \bar{\psi}\\ \bar{\theta}\end{pmatrix}=\sum_{i=1}^{4}\begin{pmatrix}1\\ L_{i}\\ M_{i}\\ N_{i}\end{pmatrix}\left[R_{i}J_{0}\left(k_{i}r\right)+S_{i}Y_{0}\left(k_{i}r\right)\right], \tag{19}$$

where $L_{i},M_{i},N_{i};(i=1,2,3,4)$ are the coupling parameters of the field functions defined below:

$$L_{i}=\frac{\Delta_{1i}}{\Delta_{i}},\quad M_{i}=\frac{\Delta_{2i}}{\Delta_{i}},\quad N_{i}=\frac{\Delta_{3i}}{\Delta_{i}};\ (i=1,2,3,4),$$

The parameters $R_i, S_i; (i = 1,2,3,4)$ are arbitrary constants which depend upon Ω and the parameters Δ_i, Δ_{1i}, Δ_{2i}, Δ_{3i}; $(i = 1,2,3,4)$ are defined in Appendix (A1.5) to (A1.8). The displacement component $\bar{u}$ is evaluated from the dilatation $\bar{e}$ in equation (19). We obtained

$$\bar{u} = \sum_{i=1}^{4} \frac{1}{k_i} \left[R_i J_1(k_i r) - S_i Y_1(k_i r) \right] \tag{20}$$

where J_0, Y_0, J_1 and Y_1 are Bessel's functions of the first and second kind of order 0 and 1, respectively.

IV. Boundary conditions

The vibration analysis of a nonlocal porous thermoelastic cylinder in the presence of rigidly fixed boundary conditions has been considered in two cases as

Case I: Rigidly fixed and thermally insulated boundary conditions

$$u(r,t) = 0, \phi(r,t) = 0, \psi(r,t) = 0, \frac{\partial \theta(r,t)}{\partial r} = 0 \text{ at } a \le r \le a\eta . \tag{21}$$

Case II: Rigidly fixed and isothermal boundary conditions

$$u(r,t) = 0, \phi(r,t) = 0, \psi(r,t) = 0, \theta(r,t) = 0 \text{ at } a \le r \le a\eta . \tag{22}$$

As mentioned earlier in governing equations, that the Eringen's differential nonlocal elasticity model has been implemented, where nonlocal effects are incorporated through modified constitutive relations, but displacement and strain fields remain unchanged. In this formulation, the boundary conditions are not directly altered by the nonlocal kernel, but are imposed on the physical displacement field. Accordingly, the rigid (clamped) boundary conditions applied to the hollow cylinder are kinematic (Dirichlet-type, Neumann Boundary Conditions) constraints and remain fully admissible within the differential nonlocal elasticity framework. The influence of non-locality is a powerful tool for both boundary-layer and localization phenomena, dependent on physical constraints such as quantum mechanics, solid mechanics, and fluid mechanics. It is observed that the nonlocal parameter leads to a smooth redistribution of the field variables rather than the formation of sharp boundary layers. The response remains globally distributed over the domain, and no evidence of mode localization is detected within the considered parameter range. This behavior is consistent with the smoothing nature of Eringen-type nonlocal elasticity.

On solving the above boundary conditions in Eqs. (21) to (22), we obtained a system of linear equations in matrix form, given below as under

$$[A]_{8\times 8}[X]_{8\times 1} = [0]_{8\times 1} \tag{23}$$

where $A = (mij)_{8\times 8}; (i, j = 1,2,3.....8)$ and $X = (R_1, R_2, R_3, R_4, S_1, S_2, S_3, S_4)^T$.

The solution (23) is an eighth-order matrix, whose constant elements are defined below:

$$m_{11}=\frac{J_1(k_1)}{k_1},\ m_{12}=\frac{J_1(k_2)}{k_2},\ m_{13}=\frac{J_1(k_3)}{k_3},\ m_{14}=\frac{J_1(k_4)}{k_4},m_{15}=-\frac{Y_1(k_1)}{k_1},\ m_{16}=-\frac{Y_1(k_2)}{k_2},$$

$$m_{17}=-\frac{Y_1(k_3)}{k_3},\ m_{18}=-\frac{Y_1(k_4)}{k_4},\ m_{31}=L_1J_0(k_1),\ m_{32}=L_2J_0(k_2),m_{33}=L_3J_0(k_3),$$

$$m_{34}=L_4J_0(k_4),m_{35}=L_1Y_0(k_1),\ m_{36}=L_2Y_0(k_2),m_{37}=L_3Y_0(k_3),m_{38}=L_4Y_0(k_4),$$

$$m_{51}=M_1J_0(k_1),m_{52}=M_2J_0(k_2),m_{53}=M_3J_0(k_3),\ m_{54}=M_4J_0(k_4),m_{55}=M_1Y_0(k_1),$$

$$m_{56}=M_2Y_0(k_2),m_{57}=M_3Y_0(k_3),m_{58}=M_4Y_0(k_4),$$

Parameters in case of thermally insulated boundary conditions;

$$m_{71}=-N_1k_1J_1(k_1),\ m_{72}=-N_2k_2J_1(k_2),m_{73}=-N_3k_3J_1(k_3),m_{74}=-N_4k_4J_1(k_4),$$
$$m_{75}=-N_1k_1Y_1(k_1),\ m_{76}=-N_2k_2Y_1(k_2),\ m_{77}=-N_3k_3Y_1(k_3),\ m_{78}=-N_4k_4Y_1(k_4),'$$

Parameters in case of isothermal boundary conditions;

$$m_{71}=N_1J_0(k_1),m_{72}=N_2J_0(k_2),m_{73}=N_3J_0(k_3),m_{74}=N_4J_0(k_4),$$
$$m_{75}=N_1Y_0(k_1),m_{76}=N_2Y_0(k_2),\ m_{77}=N_3Y_0(k_3),m_{78}=N_4Y_0(k_4),'$$

To obtain constant elements $m_{2j,}m_{4j,}m_{6j,}m_{8j}\ (j=1,2,3.....8)$, insert η along with $k_i;(i=1,2,3,4)$ in the quantities $m_{1j},m_{3j},m_{5j},m_{7j}\ (j=1,2.....,8)$.

V. Specific Scenarios

Thermoelastic cylinder with voids (single porosity):

On removing micro porosity components, i.e. $b_1=\alpha_3=\gamma=0$, and micro porosity field function is assumed to be absent, (i.e. $\psi=0$), then the analysis is simplified to a generalized thermoelastic cylinder with voids, which completely agrees with the analysis and governing equations of Sharma et al. [XV].

Elastic cylinder with voids:

On excluding thermoelastic components and thermal conductivity, i.e. $\beta_1=\beta_2=\beta_e=K=0$, along with relaxation time constants, i.e. $t_0=0$, and micro porosity function are considered to be absent, (i.e. $\psi=0$), then the analysis is simplified to an elastic cylinder with voids.

Elastic cylinder:

On excluding porosity constants, i.e. $\alpha=\alpha_1=\alpha_2=\alpha_3=b=b_1=\gamma=0$, $d=\chi_1=\chi_2=0$, thermoelastic components and thermal conductivity parameter, i.e. $\beta_1=\beta_2=\beta_e=K=0$, along with relaxation time constants, i.e. $t_0=0$. The macro and micro porosity function with specific heat parameter are assumed to be negligible, i.e. $\phi=\psi=0$, $C_e=0$, then the analysis has been reduced to the elastic

cylinder, which is completely consistent with the analysis and governing equations of Yahya and Abd-Alla [XX] in the absence of rotation parameter.

VI. Numerical results and discussion

In the present work, the analytical findings are verified through numerical simulations carried out using MATLAB software. For numerical computations, numerical constants have been taken from Pathania et al. [XIV], shown below:

$\lambda = 1.5\times10^{10}$ Nm^{-2}, $\mu = 7.5\times10^{9}$ Nm^{-2}, $\rho = 2\times10^{3}$ kgm^{-3}, $c_e = 1.809\times10^{6}$ m^{2}s^{2}K^{-1},

$\alpha_T = 1.78\times10^{-5}$ K^{-1}, $T_0 = 293$ K, $K = 1.7\times10^{2}\, W\, m^{-1}$K^{-1}, $b = 2.0\times10^{8}$ Nm^{-2},

$d = 2.1\times10^{8}$ Nm^{-2}, $\alpha_1 = 1.2\times10^{10}$ Nm^{-2}, $\alpha_2 = 2.21\times10^{10}$ Nm^{-2}, $\alpha_3 = 1.23\times10^{6}$ Nm^{-2},

$\alpha = 8.0\times10^{9}$ N, $b_1 = 8.1\times10^{6}$ N, $\chi_1 = \chi_2 = 320\, Kgm^{-1}$, $\gamma = 8.2\times10^{9}$ N, $\omega = 0.01\, Hz$,

The numerically analyzed generated data is presented in numerical complex values (frequencies) of Ω might be written as $\Omega^m = \Omega_R^m + i\Omega_I^m$. The real part has been considered as natural frequencies $\Omega_R^m = \Omega_R$, and the imaginary part is assumed as a dissipation factor $\Omega_I^m = \Omega_I$, respectively. The superscript value m in Ω^m is the mode number, which corresponds to the root of the transcendental equation, which has been obtained from a non-trivial solution of equation (23). The computer-analyzed results investigate the variations of natural frequency (Ω_R), frequency shift (f_{shift}), and thermoelastic damping (Q^{-1}) versus mode number (m).

Table 1: Natural frequencies (Ω_R) versus mode number (m) for different models GTE, TE, and E at $\varepsilon_0 = 0.75$ and $\eta = 1.35$.

S. No.	GTE	TE	E
1	0.65407	0.71595	0.68341
2	1.30415	1.25472	1.27482
3	1.53163	1.62686	1.60231
4	2.26441	2.06562	1.86441
5	2.89515	2.79886	2.14012
6	3.43523	3.20423	3.37658
7	3.66801	3.68182	3.52868
8	4.94067	4.74836	4.80679
9	5.50277	6.15592	5.37345
10	6.42168	6.66463	6.39235

Table 2: Natural frequencies (Ω_R) versus mode number (m) for different models GTE, TE, and E at $\varepsilon_0 = 0.75$ and $\eta = 1.75$.

S. No.	GTE	TE	E
1	0.77941	0.74739	0.75138
2	1.30726	1.18729	1.23528
3	1.54921	1.52761	1.50332
4	1.94797	2.29590	2.13101
5	2.78293	2.66296	2.68969
6	3.36687	3.26681	3.21886
7	4.01866	3.92268	3.77471
8	4.28661	4.31059	4.13866
9	4.86664	4.77049	4.74251
10	5.44634	5.39835	5.27838

The natural frequencies have been shown in tables for different models of thermoelasticity in fixed values of thickness and nonlocal elasticity in Tables 1 and 2. It is observed from Table 1 and Table 2 that with an increase in the value of mode number, natural frequency vibrations go on increasing for all thermoelastic models. It is to be noticed from these tables that the values predicted by the three models exhibit noticeable variations, demonstrating the influence of thermal coupling and relaxation effects incorporated in the generalized thermoelastic formulation. The field functions, such as frequency shift (f_{shift}) and thermoelastic damping (Q^{-1}) are represented graphically in Figs. 1 to 4 for fixed values of normalized thickness (η) and non-locality parameter (ε_0) with two models, such as Generalized thermoelasticity (GTE) and thermoelasticity (TE). Figs. 5 to 8 are represented for the variations of displacement, macro porosity, micro porosity, and temperature versus normalized thickness for different thermoelastic models, i.e., GTE, TE, and E.

Thermoelastic damping (inverse quality factor) (Q^{-1}) for the cases of GTE and TE has been obtained from Sharma et al. [XVII] as $Q^{-1} = 2\left|\Omega_I / \Omega_R\right|$. The frequency shift (Ω_{shift}) of a nonlocal thermoelastic hollow cylinder with double porosity material is defined as $\Omega_{shift} = \left|\dfrac{(\Omega_R^{Z^*} - \Omega_R^E)}{\Omega_R^E}\right|$ (Sharma et al. [XVII]). Here Z^* stands for generalized thermoelasticity (GTE) and thermoelasticity (TE), and Ω_R^E represents elasticity (E). The dual-porosity interaction modifies the vibrational response by reducing the effective stiffness and altering inertia through coupled macro and micro void effects. This leads to a decrease in eigenfrequencies and introduces a damping-

like attenuation behavior due to internal energy redistribution. The combined interaction produces a nonlinear frequency shift, more evident in higher modes.

Fig. 1 and Fig. 2 represent the variations of frequency shift (f_{shift}) and thermoelastic damping (Q^{-1}) with respect to mode number (m) for the GTE and TE models at $\eta = 1.35$ and $\varepsilon_0 = 0.75$. It can be depicted from Fig.1 that the frequency shift first decreases slightly and then increases significantly to achieve the peak values between $4.0 \le m \le 6.0$ and goes on decreasing, followed by dissipation. Fig. 2 illustrates that the thermoelastic damping (Q^{-1}) vibrations are larger initially, decrease to reach a dip value at $m = 2.3$, slightly increase to become linear as the value of mode number increases.

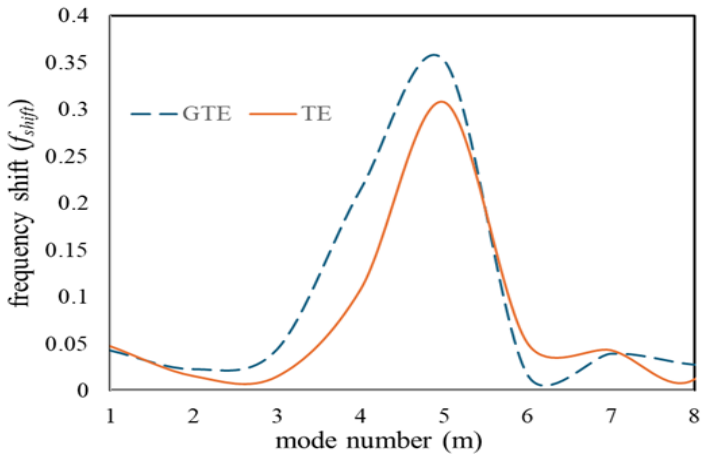

Fig. 1. Frequency shift versus mode number at $\eta = 1.35, \varepsilon_0 = 0.75$.

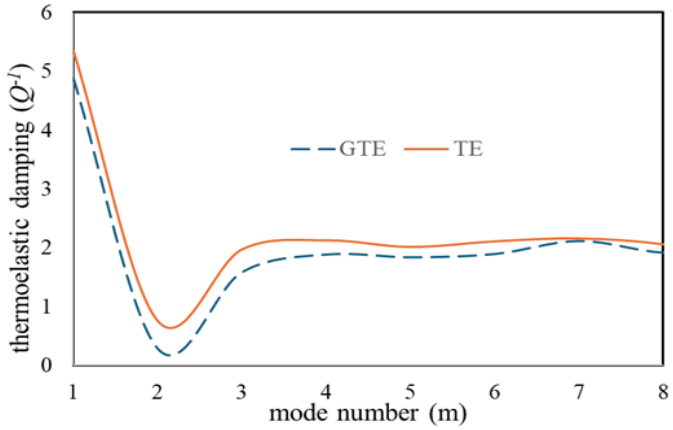

Fig. 2. Thermoelastic damping versus mode number at $\eta = 1.35$, $\varepsilon_0 = 0.75$.

It has been inferred from Fig. 3 (for $\eta = 1.35$) that frequency shift vibrations vary with low variations, and achieve peaks non-linearly for both models. A significant peak occurs around the mode number $m = 4.0$, indicating a strong thermoelastic influence at this vibration mode. Fig. 4 depicts that thermoelastic damping variations

are larger initially, decrease to reach a dip value at $m = 2.3$, increases with a rise to become linear with an increase in mode number. From all the figures, it has been observed that the GTE model has larger variations in contrast to the TE model for frequency shift variations, which follows the inequality $GTE > TE$. But thermoelastic damping indicates opposite trends, i.e., in the case of the TE model has larger variations in comparison to the GTE model of thermoelasticity. The increase and decrease in the field functions are due to coupling between mechanical and thermal effects, nonlocal components, and porosity parameters.

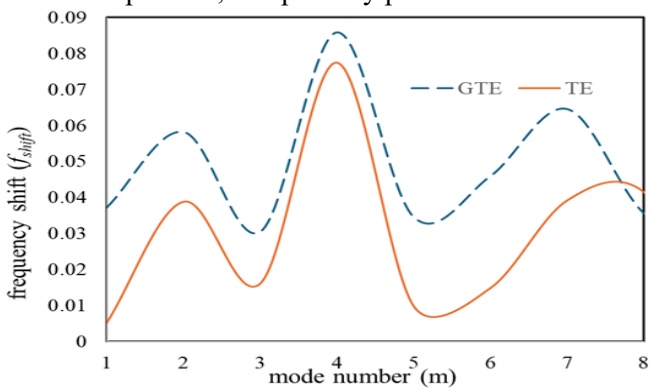

Fig. 3. Frequency shift versus mode number at $\eta = 1.75$, $\varepsilon_0 = 0.75$.

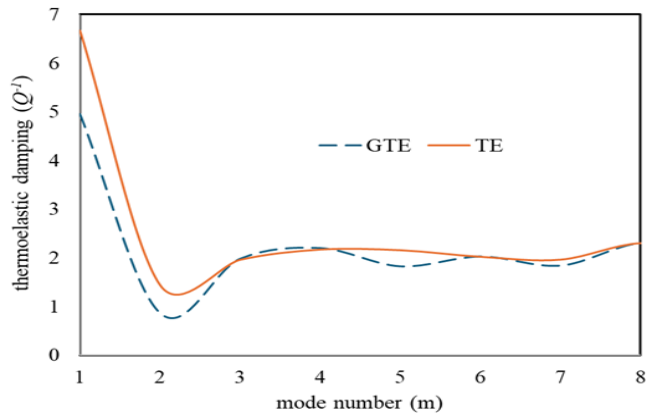

Fig. 4. Thermoelastic damping versus mode number at $\eta = 1.75$, $\varepsilon_0 = 0.75$.

Fig. 5 illustrates the variation of displacement (u) with respect to the normalized thickness (η) for three theoretical frameworks: generalized thermoelasticity (GTE), classical thermoelasticity (TE), and the purely elastic (E) model. It demonstrates the influence of thermal effects and constitutive assumptions on the mechanical response of the material. The GTE model predicts higher amplitude oscillations compared to TE and E models due to the inclusion of relaxation and non-Fourier heat conduction effects. In contrast, the elastic model shows the lowest displacement response as thermal coupling is absent. Fig. 6 presents the variation of macro porosity (ϕ) with respect to the normalized thickness (η) for three different theoretical models. The distribution exhibits a periodic oscillatory behavior through the thickness, indicating wave-like propagation of porosity in the medium under thermo-mechanical loading. It

is observed that the GTE model predicts the highest amplitude of porosity variation, followed by the TE model, while the elastic model shows the lowest response. This indicates that inclusion of thermal relaxation and non-Fourier heat conduction effects significantly enhances the porosity field response. The differences among the curves highlight the strong influence of thermoelastic coupling on void volume fraction evolution in porous structures.

Fig. 7 illustrates the variation of micro-porosity (ψ) across the normalized thickness (η) for three different models. The distribution exhibits a periodic oscillatory nature, indicating wave-like behavior of microstructural voids within the material under thermo-mechanical loading. It is observed that the GTE model predicts the highest magnitude of micro-porosity variation, followed by the TE model, while the elastic model shows the lowest response throughout the thickness. This difference clearly highlights the significant role of thermal effects and relaxation phenomena in influencing microstructural deformation. The inclusion of non-Fourier heat conduction in the TE model and thermal coupling in the GTE model leads to enhanced porosity fluctuations compared to classical elasticity.

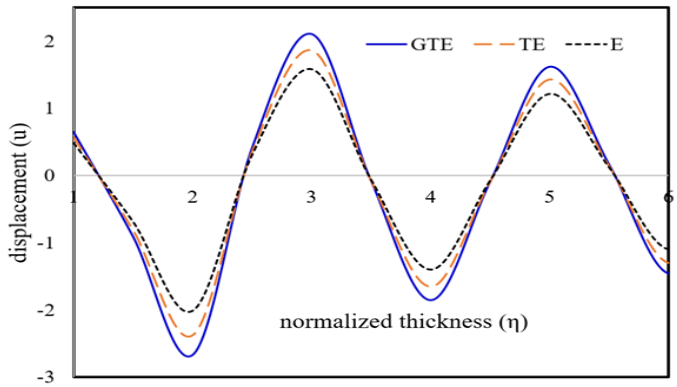

Fig. 5. Displacement versus normalized thickness for different thermoelastic models.

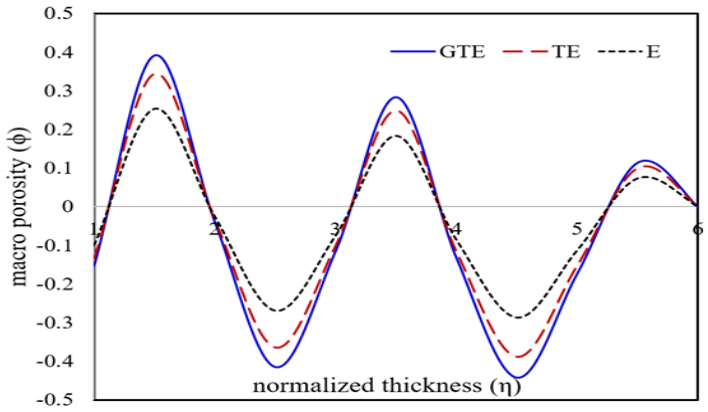

Fig. 6. Macro porosity versus normalized thickness for different thermoelastic models.

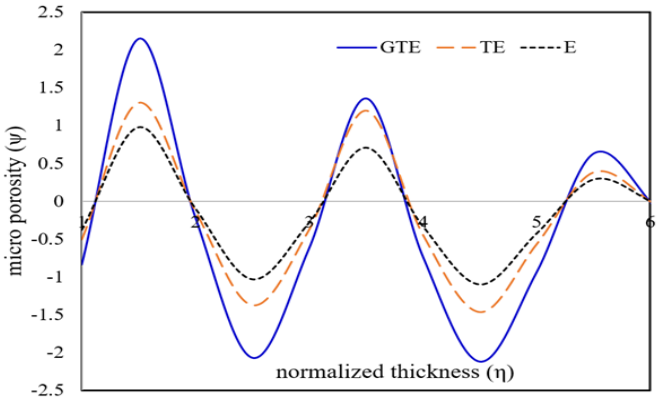

Fig. 7. Micro porosity versus normalized thickness for different thermoelastic models.

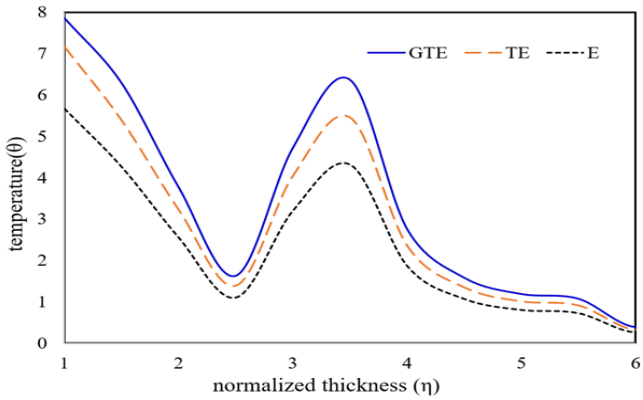

Fig. 8. Temperature versus normalized thickness for different thermoelastic models.

The variation of temperature (θ) across the normalized thickness (η) for three different theoretical models has been illustrated in Fig. 8. The temperature distribution shows a nonlinear, oscillatory-like decay along the thickness, indicating the influence of thermo-mechanical coupling in the medium. It is observed that the GTE model predicts the highest temperature values throughout the domain, followed by the TE model, while the elastic model exhibits the lowest temperature response. The pronounced difference between the curves highlights the significant role of thermal relaxation effects and non-Fourier heat conduction in the generalized thermoelastic framework. The increasing nonlocality leads to smoother and more delocalized mode shapes due to the intrinsic length-scale effect, while higher thickness ratios enhance radial stiffness and modify the oscillation distribution across the cylinder wall. In particular, higher modes show greater sensitivity, with noticeable redistribution of radial displacement and coupled field intensities. Lower-order modes are primarily displacement-dominated, whereas intermediate and higher modes exhibit increasing coupling with thermal and porosity fields. In particular, certain modes show stronger thermal influence due to enhanced heat diffusion effects, while others are more significantly affected by porosity interactions arising from macro–micro void coupling.

VII. Conclusions

Trends in both tables reveal that an increase in the behavior of natural frequencies with respect to mode number has been observed in the progression from top to bottom in the tables. Figures indicated that the variations in frequency shift follow the inequality $GTE > TE$, in contrast to thermoelastic damping, which follows the inequality $GTE < TE$. The tables and figures inferred that fluctuations in the behavior of functions that there is coupling between volume fractions of void, mechanical forces, and thermal effects. By understanding the double porous thermoelastic cylindrical structure introduces stress and thermal variations, and researcher may develop reliable and stronger components, developing performance of mechanical systems.

Appendix

$$A_1 = \begin{pmatrix} b_{44} - b_{33} - b_{22} - B^* B_1^* b_{44} + B^* b_{32} - B_1^* b_{23} - b_{11} + B^* B_1^* b_{11} \\ -b_{12}b_{21} + B^* b_{12}b_{31} - b_{13}b_{31} + b_{14}b_{11} + B^* B_1^* b_{14}b_{41} \end{pmatrix}, \quad \text{(A1.1)}$$

$$B_1 = \begin{pmatrix} b_{33}b_{44} - b_{34}b_{43} + b_{22}b_{44} + B^* b_{32}b_{44} - b_{22}b_{33} + B^* b_{34}b_{43} + \\ B_1^* b_{23}b_{44} - b_{23}b_{32} + B_1^* b_{24}b_{43} + b_{24}b_{42} + b_{44}b_{11} - b_{11}b_{33} - \\ b_{11}b_{22} - B^* B_1^* b_{11}b_{32} - B_1^* b_{23}b_{11} + b_{12}b_{21}b_{44} - b_{12}b_{21}b_{33} - \\ B^* b_{31}b_{44}b_{12} + B^* b_{12}b_{34}b_{41} - b_{12}b_{23}b_{31} - b_{12}b_{41} - B_1^* b_{13}b_{21} \\ -b_{13}b_{21} + b_{13}b_{34}b_{41} - b_{13}b_{22}b_{31} - B_1^* b_{13}b_{24}b_{41} + b_{13}b_{31}b_{44} + \\ B_1^* b_{14}b_{21}b_{43} + b_{14}b_{12} - b_{14}b_{31}b_{43} - b_{14}b_{41}b_{33} - b_{14}b_{22}b_{41} + \\ B^* b_{14}b_{31}b_{42} - B^* b_{14}b_{41}b_{32} - B_1^* b_{14}b_{23}b_{41} \end{pmatrix}, \quad \text{(A1.2)}$$

$$C_1 = \begin{pmatrix} b_{22}b_{33}b_{44} - b_{22}b_{34}b_{43} - b_{23}b_{33}b_{44} - b_{23}b_{34}b_{43} - b_{24}b_{32}b_{43} \\ -b_{24}b_{33}b_{42} - b_{11}b_{33}b_{44} + b_{11}b_{34}b_{43} + b_{11}b_{22}b_{44} - b_{11}b_{22}b_{33} + \\ B^* b_{11}b_{32}b_{44} + B^* b_{11}b_{34}b_{43} + B_1^* b_{11}b_{23}b_{44} - b_{11}b_{23}b_{32} + B_1^* b_{11}b_{24}b_{43} \\ +b_{11}b_{24}b_{42} + b_{12}b_{21}b_{33}b_{44} - b_{12}b_{21}b_{34}b_{43} + b_{12}b_{23}b_{31}b_{44} - b_{12}b_{23}b_{34}b_{44} \\ +b_{12}b_{24}b_{31}b_{43} - b_{12}b_{33}b_{41} + b_{13}b_{21}b_{32} + b_{13}b_{21}b_{44} + b_{13}b_{22}b_{31}b_{44} + \\ b_{13}b_{22}b_{34}b_{41} - b_{13}b_{24}b_{31}b_{42} + b_{13}b_{24}b_{41}b_{32} - b_{14}b_{21}b_{32}b_{43} + b_{14}b_{33}b_{42} \\ -b_{14}b_{22}b_{31}b_{43} - b_{14}b_{22}b_{31}b_{41} - b_{14}b_{23}b_{31}b_{42} + b_{14}b_{23}b_{32}b_{41} \end{pmatrix}, \quad \text{(A1.3)}$$

$$D_1 = \begin{pmatrix} b_{11}b_{22}b_{33}b_{44} - b_{11}b_{22}b_{34}b_{43} - b_{11}b_{22}b_{32}b_{44} - b_{11}b_{23}b_{34}b_{43} \\ -b_{11}b_{24}b_{32}b_{43} - b_{11}b_{24}b_{33}b_{42} \end{pmatrix}, \quad \text{(A1.4)}$$

$$\Delta_i = \begin{vmatrix} b_{12}k^2 & b_{13}k^2 & b_{14}k^2 \\ k^2+b_{22} & B^*k^2-b_{23} & b_{24} \\ B^*k^2-b_{32} & k^2+b_{33} & b_{34} \end{vmatrix}; \ (i=1,2,3,4), \tag{A1.5}$$

$$\Delta_{1i} = \begin{vmatrix} -\left(k^2+b_{11}\right) & b_{13}k^2 & b_{14}k^2 \\ b_{21} & B^*k^2-b_{23} & b_{24} \\ b_{31} & k^2+b_{33} & b_{34} \end{vmatrix}; \ (i=1,2,3,4), \tag{A1.6}$$

$$\Delta_{2i} = \begin{vmatrix} b_{12}k^2 & -\left(k^2+b_{11}\right) & b_{14}k^2 \\ k^2+b_{22} & b_{21} & b_{24} \\ B^*k^2-b_{32} & b_{31} & b_{34} \end{vmatrix}; \ (i=1,2,3,4), \tag{A1.7}$$

$$\Delta_{3i} = \begin{vmatrix} b_{12}k^2 & b_{13}k^2 & -\left(k^2+b_{11}\right) \\ k^2+b_{22} & B^*k^2-b_{23} & b_{21} \\ B^*k^2-b_{32} & k^2+b_{33} & b_{31} \end{vmatrix}; \ (i=1,2,3,4). \tag{A1.8}$$

Conflict of Interest:

There was no relevant conflict of interest regarding this paper.

References

I. Achenbach J. D., Wave propagation in elastic solids, (North Holland Publishing Co. New York 1973).

II. Ciarletta M. and Sumbatyan M.A., Reflection of plane waves by the free boundary of a porous elastic elastic half-space, J. Sound Vib. **259** (2), 253-264 (2003). 10.1006/jsvi.2002.5149

III. Cowin S. C. and Nunziato J. W., Linear elastic materials with voids, J. Elasticity **13**, 125-147 (1983). 10.1007/BF00041230

IV. Dhaliwal R.S. and Singh A., Dynamical coupled thermoelasticity (Hindustan Publ. Delhi, 1980).

V. Eringen A. C., Theory of nonlocal thermoelasticity, Int. J. Eng. Sci. **12**, 1063-1077 (1974). 10.1016/0020-7225(74)90033-0

VI. Ewing W. M., Jardetzky W. S. and Press F., Elastic waves in layered media, (Mc-Graw-Hill Book Company Inc. New York 1957).

VII. Gupta S., Dutta R. and Das S., Memory responses in a nonlocal micropolar double porous thermoelastic medium with variable conductivity under Moore-Gibson-Thompson thermoelasticity theory, J. Ocean Eng. Sci. **8**(3), 263-277 (2023). 10.1016/j.joes.2022.01.010

VIII. Iesan D. and Quintanilla R., On a theory of thermoelastic materials with a double porosity structure, J. Therm. Stresses **37** (9), 1017-1036 (2014). 10.1080/01495739.2014.914776

IX. Iesan D., A theory of thermoelastic materials with voids, Acta Mech. **60**, 67-89 (1986). 10.1007/BF01302942

X. Ismail G. M., Elidy E. S., Mahdy A. M. S., Tantawi R. S. and Lotfy K., Nonlocal thermoelastic response of semiconductor media with double porosity under photothermal excitation, Int. J. Mech. Mater. Des. **22**, 70 (2026). 10.1007/s10999-026-09873-w

XI. Kansal T., The theory of thermoelasticity with double porosity and microtemperatures, Comput. Methods Sci. Technol**,**28 (3), 87-107 (2022). 10.12921/cmst.2022.0000016

XII. Lord H.W., Shulman Y, A generalized dynamical theory of thermoelasticity. J. Mech. Phys. Solids 15(5), 299-309 (1967). 10.1016/0022-5096(67)90024-5

XIII. Parra C. C., Venegas R. and Zieliński T.G. , Acoustic wave propagation in double-porosity permo-elastic media, Appl. Math. Mech. **46**, 1511-1532 (2025). 10.1007/s10483-025-3281-8

XIV. Pathania V., Kumar R., Gupta V., Barak M.S., Generalized plane waves in a rotating thermoelastic double porous solid,Int. J. Appl Mech. Engg., 27(4): 138-154 (2022). 10.2478/ijame-2022-0055

XV. Sharma D. K., Thakur P. C., Sarkar N. and Bachher M., Vibrations of a nonlocal thermoelastic cylinder with void. Acta Mech. **231**, 2931-2945 (2020). 10.1007/s00707-020-02681-z

XVI. Sharma D.K., Rana N., Sarkar N., Transient response of a nonlocal viscoelastic cylinder with double porosity, Mech. Solids, 58: 1912–1927(2023). 10.3103/S0025654423600964

XVII. Sharma J.N., Sharma P.K., Mishra K.C., Analysis of free vibrations in axisymmetric functionally graded thermoelastic cylinders. Acta Mech 225,1581-1594 (2014). 10.1007/s00707-013-1010-3

XVIII. Sharma V., Sharma D. K. and Sarkar N., Analysis of an axisymmetric cylinder with variable thermal conductivity and point loads in semi-infinite medium via the Moore-Gibson-Thompson Model of thermoelasticity, Int. J. Theor. Phys. **64**, 231 (2025). 10.1007/s10773-025-06098-z

XIX. Svanadze M., Fundamental solutions in the linear theory of consolidation for elastic solids with double porosity, J. Math. Sc. **195**, 258-268 (2013). 10.1007/s10958-013-1578-0

XX. Yahya G. and Abd-Alla A., Radial vibrations in an isotropic elastic hollow cylinder with rotation. J. Vib. Control. **22(**13), 3123-3131(2016). 10.1177/1077546314560001

XXI. Yildirim E. and Esen I., Effect of the porous structure on the hygrothermal vibration analysis of functional graded nanoplates using nonlocal high-order continuum plate model, Acta Mech. 235, 5079-5106 (2024). 10.1007/s00707-024-03990-3

XXII. Zhong H., Zhang W., Yin H. and Liu H., Study on mechanism of viscoelastic polymer transient flow in porous media, Geofluids 8763951 (2017). 10.1155/2017/8763951